Title
Quantitative long-term measurements of burns in a rat model using Spatial Frequency Domain Imaging (SFDI) and Laser Speckle Imaging (LSI).

Journal
Lasers in surgery and medicine, 49(3)

ISSN
1096-9101

Authors
Ponticorvo, Adrien
Burmeister, David M
Rowland, Rebecca
et al.

Publication Date
2017-03-21

HHS Public Access

Author manuscript

Lasers Surg Med. Author manuscript; available in PMC 2018 March 01.

Published in final edited form as:

Lasers Surg Med. 2017 March ; 49(3): 293–304. doi:10.1002/lsm.22647.

Quantitative long term measurements of burns in a rat model using Spatial Frequency Domain Imaging (SFDI) and Laser Speckle Imaging (LSI)

Adrien Ponticorvo[1], **David M. Burmeister**[2], **Rebecca Rowland**[1], **Melissa Baldado**[1], **Gordon T. Kennedy**[1], **Rolf Saager**[1], **Nicole Bernal**[3], **Bernard Choi**[1,4], and **Anthony J. Durkin**[1,*]

[1]Beckman Laser Institute and Medical Clinic, University of California, Irvine, 1002 Health Sciences Road East, Irvine, CA 9261 7

[2]United States Army Institute of Surgical Research, 36950 Chambers Pass, Fort Sam Houston, TX, 78234

[3]UC Irvine Regional Burn Center, Department of Surgery, 333 City Boulevard West, Suite 705, Orange, CA 92868

[4]Department of Biomedical Engineering, University of California, Irvine, 3120 Natural Sciences II, Irvine, CA 92697

Abstract

The current standard for diagnosis of burn severity and subsequent wound healing is through clinical examination, which is highly subjective. Several new technologies are shifting focus to burn care in an attempt to help quantify not only burn depth but also the progress of healing. While accurate early assessment of partial thickness burns is critical for dictating the course of treatment, the ability to quantitatively monitor wound status over time is critical for understanding treatment efficacy. SFDI and LSI are both non-invasive imaging modalities that have been shown to have great diagnostic value for burn severity, but have yet to be tested over the course of wound healing. In this study, a hairless rat model (n=6, 300-450g) was used with a four pronged comb to create four identical partial thickness burns (superficial n=3 and deep n=3) that were used to monitor wound healing over a 28 day period. Weekly biopsies were taken for histological analysis to verify wound progression. Both SFDI and LSI were performed weekly to track the evolution of hemodynamic (blood flow and oxygen saturation) and structural (reduced scattering coefficient) properties for the burns. LSI showed significant changes in blood flow from baseline to 220% in superficial and 165% in deep burns by day 7. In superficial burns, blood flow returned to baseline levels by day 28, but not for deep burns where blood flow remained elevated. Smaller increases in blood flow were also observed in the surrounding tissue over the same time period. Oxygen saturation values measured with SFDI showed a progressive increase from baseline values of 66% to 74% in superficial burns and 72% in deep burns by day 28. Additionally, SFDI showed significant decreases in the reduced scattering coefficient shortly after the burns were created. The scattering coefficient progressively decreased in the wound area, but returned towards baseline conditions at the end of the 28 day period. Scattering changes in the surrounding tissue remained

* adurkin@uci.edu, Phone: 949-824-3284, Fax: 949-824-8413.

constant despite the presence of hemodynamic changes. Here we show that LSI and SFDI are capable of monitoring changes in hemodynamic and scattering properties in burn wounds over a 28 day period. These results highlight the potential insights that can be gained by using noninvasive imaging technologies to study wound healing. Further development of these technologies could be revolutionary for wound monitoring and studying the efficacy of different treatments.

1. Introduction

The incidence of burns severe enough to warrant medical attention has been measured as high as 11 million people annually worldwide [1] with the sequelae of non-fatal burns often severe enough to cause permanent disability. Burn wounds and the subsequent scarring have damaging effects to tissue both cosmetically and functionally, necessitating the search for better and more efficient treatments. One challenging aspect of burn wound care is monitoring the progress of wound healing amid a host of surrounding physiological changes. A number of mechanisms are involved in the process of burn wound progression, including local tissue hypoperfusion, edema, prolonged inflammation, angiogenesis and changes in collagen organization[2]. Complicating matters is the fact that burn injuries are not static but can continue to worsen over the course of several days[3,4]. Delays in diagnosis and subsequent treatment can allow for burn wounds to spread and affect a larger volume of tissue[5]. Despite the clinical significance of being able to understand and monitor the progression of burn wounds, it remains a poorly understood phenomenon mostly assessed via visual diagnosis[5,6].

Imaging technologies have become more prevalent in clinical burn research in an attempt to better understand and quantify the physiological changes associated with burn wounds. Laser Doppler imaging (LDI) has become a standard alongside clinical evaluation, and more recently thermographic and spectroscopic techniques have become more common[7-9]. The majority of research in this area has focused on predicting the outcome of burn wounds so that interventions, if needed, can be done sooner. While important, less work has been done using imaging techniques to quantify burn wound progression and healing. Such quantification would be a useful tool for testing the efficacy of new treatment options. Recent papers using imaging techniques such as Indocyanine green (ICG) dye angiography[10] and active dynamic thermography (ADT)[11] in conjunction with LDI to study burn wound conversion have shown that there are structural changes in burn wound progression that cannot be detected by analyzing only physiological blood flow changes. Other techniques such as terahertz spectroscopy that are sensitive to water content in addition to some structural elements of tissue have shown promise for monitoring burn wounds[12]. Being able to track these structural changes over time could provide novel insights for understanding burn wound progression and healing.

Spatial Frequency Domain Imaging (SFDI) is a non-contact imaging technique that can be used to determine the optical properties of tissue and is sensitive to both hemodynamic and structural changes[13,14]. While earlier research utilized SFDI to study its predictive capabilities and the acute physiological impact of burns in rats and pigs[15,16], to date no

studies have used this technology for the long term monitoring of burn wound progression. Laser speckle imaging (LSI) is a technique similar to LDI that measures fluctuations of a static speckle pattern on a tissue surface to generate images of blood flow. Because LSI uses diffuse laser light to create the speckle pattern, there is no need to scan a light source to generate images leading to faster acquisition times. This makes LSI well suited to avoid confounding factors such as small motion artifacts due to breathing.

These non-invasive imaging techniques have been used to aid the clinical diagnosis of burn severity (e.g., depth of the burn) which is ultimately important for predicting the course of wound healing[8]. However, monitoring the dynamic process of wound healing across time with these imaging techniques is a promising strategy[17]. Specifically, it is reasonable to hypothesize that changes in tissue perfusion and connective tissue content would likely be reflected in values of LSI and SFDI, respectively. To this end, LSI has been shown to measure hemodynamic changes during wound healing in the ears of mice[18]. This is further evidenced in another study in pediatric scald burns showing initial perfusion related to duration of healing out to 14 days[19]. Similarly, after the peak of angiogenesis in wound healing, collagen deposition in the proliferative phase can affect scar formation, which may also be assessed with imaging techniques[20]. While these imaging technologies hold great promise for assessment of wounds across time, their full potential remains unknown.

In order to fully characterize the physiological parameters measured by SFDI and LSI during burn wound progression, we examined the performance of these techniques in a controlled rat burn model over a 28 day period.

2. Methodology

2.1 Spatial Frequency Domain Imaging (SFDI)

The SFDI measurements were performed with a custom made device described previously[21]. A 250 W quartz tungsten halogen lamp (Newport Oriel, Stratford, CT) was used to project diffuse white light with a spectral irradiance of approximately 70 mW m^{-2} nm^{-1} over a measured field of view of 0.09 × 0.066 m^2. That light was reflected off a digital micromirror device (DMD) (Texas Instruments, Dallas, TX) used to create arbitrary spatial patterns. The pattern alternated between a sinusoidal spatial frequency of 0.2 mm^{-1} and diffuse light with no pattern. The reflected light from the sample was captured using a Nuance™ camera system (CRI Inc., Woburn, MA), which combines a 12-bit CCD camera and a liquid crystal tunable filter (λ = 650–1100 nm, FWHM = 10 nm). This system was used to collect images at 17 equally spaced wavelengths between 650 and 970 nm. The exposure time of the camera was adjusted at each wavelength to utilize the full dynamic range of the camera while ensuring no saturation. Exposure times typically ranged between 40 – 900 milliseconds. Crossed linear polarizers were used in the illumination and detection arms. A NIR linear polarizer (Meadowlark Optics, Frederick, CO) was placed after the projection lens, and the first stage of the Nuance camera system acted as the second polarizer. This arrangement was employed to minimize the impact of specular reflection.

At every wavelength, the optical properties (reduced scattering and absorption coefficients) of the measured tissue were determined by fitting the collected imaging data to a look-up-

table for scattering and absorption at both spatial frequencies generated by a forward Monte Carlo simulation[22]. A least squares linear fit algorithm was used to transform the absorption coefficient values into concentrations of oxygenated hemoglobin (HbO_2), deoxygenated hemoglobin (Hb) and water fraction (H_2O). Tissue oxygen saturation (stO_2) was subsequently calculated by dividing HbO_2 by the sum of HbO_2 and Hb[23].

2.2 Laser Speckle Imaging (LSI)

Laser speckle images were acquired from the same region of interest using the CCD camera with which SFDI data was acquired. This was done immediately after the SFDI measurements were completed. An 809 nm collimated laser (Ondax, Monrovia, CA) was used to illuminate the tissue surface. For each measurement, 50 raw speckle images were collected at a 10 ms exposure time. The LSI device did not require any calibration to analyze results as has been shown previously[24]. MATLAB was again used to collect the raw images from the camera. The raw speckle images were converted into speckle contrast images and subsequently speckle flow index (SFI) maps as described previously[25,26]. Relative changes in SFI were assumed to be equivalent to relative changes in blood flow[27,28]. Baseline measurements for both imaging techniques were made shortly before the burns were created and day 0 measurements took place one hour after the burn. Follow up imaging was performed on days, 7, 14, 21, and 28 days post-burn.

2.3 Animals

Male CD Hairless rats (Charles River Laboratories Inc., San Diego, CA, n=6) were used in this experiment. These were chosen because they are euthymic and do not exhibit the typical characteristics of hair growth/regrowth found in other hairless rats, making them well suited to wound healing studies. Based on the experience that we gained in our previous rat burn investigation[29], we chose to work with rats weighing between 300 and 450 g. In this weight range, there is adequate skin on which to place the burn tool in good thermal contact. In addition, rats of this size appear to be relatively stable in weight over the 28 day time course of the investigation, despite the presence of burn wounds. Each rat was depilated with Nair (Church and Dwight, Princeton, NJ) three days before experimentation began. All experiments were approved by the UC Irvine Institutional Animal Care and Use Committee (IACUC #1999-2064).

On the first day of experimentation, rats were anesthetized with an intraperitoneal injection of ketamine (87 mg/kg) and xylazine (13 mg/kg). During all subsequent measurement days, the snout of each rat was inserted to a nosecone that delivered isoflurane (2%). At the completion of imaging on the 28th day, rats were euthanized with sodium pentobarbital (150 mg/kg).

2.4 Creation of controlled, graded burn wounds

As was done in our previous investigation on acute burns, to generate repeatable partial thickness burns, a heated 313g “brass comb” was used[24,29]. The comb is made up of four 1×2 cm^2 tines separated by 0.5 cm gaps. Before the experiment, the comb was heated to 100 °C in an Isotemp dry bath incubator (Thermo Fisher Scientific Inc.) (Fig. 1b). The heated comb was applied to the dorsum of the rats for 4 seconds to produce superficial burns

(n=3), and for 8 seconds to produce deep burns (n=6). The weight of the comb due to gravity was the only force used to apply the brass probe, and no additional pressure was applied to the comb.

2.5 Histopathology

Tissue samples were taken from one of the four burned regions of the anesthetized animal after the imaging was completed on 0, 7, 14, and 28 days post-burn (Fig. 1c). A 5 mm circular punch biopsy was excised from the center of the burn. Due to the perturbation of the burn wound region caused by this process, only burns that were biopsied on day 28 were included in the final LSI and SFDI results. The tissue was fixed in a 10% buffered formalin solution for 24 hours and embedded in paraffin wax blocks. Slices 6 μm thick were sectioned and stained with Mayer's Hematoxylin and Eosin. The mounted tissue sections were examined for collagen coagulation, hair follicle damage, and reepithelization to determine burn depth and wound healing[30].

2.6 Color Photography

Color images were taken in a fixed geometry with a 14-megapixel digital camera (NEX-3, Sony Corporation of America, New York, NY) after each SFDI/LSI measurement.

2.7 Statistical Analysis

For each animal, both a region of interest (ROI) within the burn wound and a normal control region approximately 3 cm away from the burns were selected. For burns where the eschar had partially fallen off, care was taken to choose an ROI within the burn but outside the eschar. If the eschar covered the entire wounded area then the ROI was selected over the eschar. For each burn category (superficial partial thickness and deep partial thickness burns) a student's t-test was used to assess differences in measured parameters relative baseline conditions. A p-value less than 0.05 was considered statistically significant for this study, and these values are marked with an * in tables and graphs. The parameter values from each region were averaged across burns of the same severity and are shown in Table 1 as well as various time course plots.

3. Results

3.1 Color Images

Color image examples from two experiments are shown in Fig. 2. Eschar formation was typically apparent by day 7 on both superficial and deep burns. By day 14, this eschar was typically absent or, at minimum, smaller in the superficial burns when compared to the deep burns.

3.2 Histological Analysis

Burn wound depth and morphology was established through analysis of histological images. Representative histological images for baseline, 0, 7, 14, and 28 days post-burn are shown in Fig. 3. Measurement of day 0 biopsies showed that the superficial burns did not extend past the sebaceous glands, indicating that they were superficial partial thickness burns. The deep

burns extended further, damaging more follicular structures. On average, the superficial burns penetrated 350 μm, whereas the deep burns reached 550 μm in these day 0 biopsies. On day 7, significantly more eschar is seen in the deeper wounds than in superficial wounds. The average thickness of the eschar observed in the day 7 biopsies was 320 μm in the superficial burns and 540 μm in the deep burns. Moreover, superficial wounds re-epithelialized more quickly, with a largely hyperplastic epithelium present on day 7, not apparent in the deeper burns. On days 14 and 28, this epithelium gradually returns to baseline thickness only in the superficial burn group, and remains slightly hyperplastic in the deep burns.

3.3 LSI measured blood flow changes

The average time course of relative blood flow changes are shown in Fig. 4a. There was a statistically significant decrease in both superficial (60%) and deep burns (64%) at one hour after the initial burn. At day 7 there was a statistically significant increase in superficial partial thickness burns (220%) before decreasing and returning closer to baseline values over the next three weeks. At day 7 there was also a statistically significant increase in deep partial thickness burns (166%) but this increase continued through day 14 (210%) before decreasing towards baseline values. By day 28, the blood flow values for deep burns, but not superficial burns, were still significantly higher (154%) than baseline values.

SFI images taken from a representative rat for each burn severity are depicted in Fig. 4b. The decrease in blood flow in the burned region on day 0 following the burn can clearly be seen as well as the increased flow on the following timepoints. In addition to the changes in blood flow seen in the burned regions, the images highlight the general increase in blood flow seen in the surrounding area in the days following the burn, representing the burn zone of hyperemia. The image for the deep partial thickness burn on day 14 also highlights the confounding effects of the aging burn eschar as there is reduced flow in that region but increased flow underneath.

3.4 SFDI measured deoxygenated hemoglobin

A time course of average chromophore concentrations for deoxygenated hemoglobin is shown in Fig. 5a. Deoxygenated hemoglobin baseline values (37 μM) in superficial partial thickness burns showed a statistically significant increase shortly after the burn (41 μM) that continued at day 7 (43 μM) before returning closer to baseline values by day 14. Similarly for deep partial thickness burns, deoxygenated hemoglobin values were significantly above baseline values on days 7 (45 μM) and 14 (46 μM) before gradually decreasing towards baseline values on days 21 and 28. There was also a trend of decreasing deoxygenated hemoglobin in the surrounding normal regions over the course of the experiment. Images of deoxygenated hemoglobin concentration for a typical experiment at each time point are shown in Fig. 5b.

3.5 SFDI measured oxygen saturation changes

A time course of oxygen saturation values for superficial and deep burns is shown in Fig. 6a. There were no statistically significant changes in baseline oxygen saturation (66%) for either group shortly after the burn. But by day 21 where there were significant increases in

superficial (74%) and deep (72%) burns that continued at day 28. There was also a trend of increasing oxygen saturation in the surrounding normal regions over the course of the experiment. Corresponding images of oxygen saturation values for a typical experiment are shown in Fig. 6b.

3.6 SFDI measured reduced scattering changes

Time courses of reduced scattering values (μ_s') at 650 nm for superficial and deep burns are displayed in Fig. 7a. While the reduced scattering coefficient is calculated at multiple wavelengths for both categories of burns, there were no changes to the trends of the time course data regardless of the wavelengths chosen. Furthermore there were no changes in the statistical significance of the data regardless of the wavelengths chosen. In order to simplify the presentation of the data, only the 650 nm data is shown. Baseline μ_s' values for superficial (2.18 mm^{-1}) and deep (2.10 mm^{-1}) burns were similar, but decreased after the creation of the burn in both populations with a statistically significant decrease (1.66 mm^{-1}) for deep burns. By day 7 there was a statistically significant decrease in μ_s' for both superficial (1.34 mm^{-1}) and deep (1.23 mm^{-1}) burns. In superficial burns μ_s' began to steadily increase towards baseline conditions starting at day 14 (1.73 mm^{-1}) through day 28 (1.94 mm^{-1}) although values remained significantly below baseline values even at day 28. In deep burns, μ_s' values continued to decrease at day 14 (1.21 mm^{-1}) before steadily returning closes to baseline values on days 21 (1.47 mm^{-1}) and 28 (1.84 mm^{-1}). In contrast, μ_s' values in the normal regions remained consistent over the course of the experiment. Images depicting reduced scattering changes for a typical experiment are shown in Fig. 7b.

3.7 SFDI measured water fraction

The average time courses for water fraction values are shown in Fig. 8a. There were no statistically significant changes of the water fraction in superficial burns. However, there was a trend of increased water fraction values in the burned region over the 28 days while values in the normal regions remained unchanged. There was a statistically significant increase in the water fraction of deep burns on day 14 (65%) compared to baseline values (45%). Similar to superficial burns, there was also a trend of increased values throughout the 28 day period compared to baseline values. Representative images of the water fraction taken from a superficial and deep burn are depicted in Fig. 8b.

3.8 Summary

Table 1 below summarizes the LSI and SFDI results.

4. Discussion

4.1 Histology

The burn method used in this experiment was a combination of a burn comb[24,29] and incubator[16] used independently in previous burn wound experiments. This combination created burns of known and repeatable burn thicknesses corresponding to superficial and deep second degree burns. Previous rat studies reported similar burn depth severity, confirming the repeatability of this burn method[29].

One week post-burn, eschar formation is apparent, with greater eschar area and thickness in deep burns as shown with macroscopic pictures (Fig. 2) and histology (Fig. 3) respectively. Differing levels of re-epethelialization are also present between the different burn severities. In the deep burns, reepethelialization emanates from the hair follicle, showing the level of damage to the bulge. In the superficial partial burns, the layer of reepitheliatized skin covers the area between scab and dermis, having originated from an intact hair follicle bulge.

Two weeks post burn, scar tissue is present in more abundance in deeper burns, while hair follicles are more abundant in the superficial burn scar regions. The new epidermis has become anchored to the top layer of scar tissue. Four weeks post-burn, the level of mature collagen is closer to the epidermis of the superficial partial sample compared to the deep partial sample.

As one of the gold standards for determining burn severity and monitoring wound healing, histologic observations show detailed changes within the tissue. Besides the initial difference in burn depth, the level of reepithelialization on day 7 differs greatly between the two burn severities. Regrowth of hair follicles also occurs at a later timepoint in the deep partial thickness burns in comparison to the superficial partial thickness burns. From a clinical standpoint, while histology represents an unequivocal way to determine burn depth, taking and processing biopsies is an extremly invasive and time consuming procedure.

4.2 Laser Speckle Imaging

There was a significant initial decrease in blood flow after the burn injury in both groups of burns. Previous experiments with a similar rat burn model also detected decreases in flow shortly after injury[24]. Several experiments in pig burn models have also seen significant decreases in blood flow that are proportional with the severity of the burn[16,31]. Across all of these studies the decrease in blood flow for partial thickness burns range in values between 15 and 50% which is consistent with the initial changes in blood flow seen here. The increase in blood flow seen by day 7 for the superficial (220%) and deep (166%) burns is consistent with other groups that see blood flow begin to progressively increase around day 7 for partial thickness burns in a pig model[31]. By day 14 blood flow in the superficial burns was returning toward baseline values while blood flow in the deep partial thickness burn continued to increase (210%). As increased blood flow is a common indicator of wound healing[32,33], this difference highlights the longer times needed for deeper burns to progress through wound healing and the ability to monitor that progression with LSI. By day 28, blood flow in the deep burns is still significantly higher than baseline conditions (154%) (Fig. 4a).

Another benefit of imaging technologies like LSI over point-based measurements such as laser Doppler flowmetry is the ability to account for the tissue heterogeneity associated with eschar formation around day 14 (Fig. 4b). The eschar layer that formed over the burn wounds from day 7 onward did obscure some of the speckle flow data. Regions of interest were chosen with this in mind, focusing on areas of the burn where the scab was thin enough to allow for the measurement of the living tissue beneath.

4.3 Deoxygenated Hemoglobin and Oxygen Saturation

In these experiments we found an increase in deoxygenated hemoglobin at early time points in superficial and deep burns. Previous experiments using a similar rat burn model have shown acute increases in deoxygenated hemoglobin for deep burns[29]. Studies in mice[34] and pig burn models[35] have also shown increases in deoxygenated hemoglobin over a 72 hour period. Here we have characterized the changes in deoxygenated hemoglobin at time points that are well past the early inflammation stages of wound healing and into the later proliferation and maturation stages. We see that deoxygenated hemoglobin returns towards baseline values by the end of the 28 day period but this change occurs more quickly in the superficial burns. Interestingly, the deoxygenated hemoglobin values by day 28 in the burned area and the surrounding tissue were below baseline values. Combined with the information of increased oxygen saturation and blood flow, there is an implication of increased metabolism in these areas. The normal regions also show increases in oxygen saturation by the end of the 28 day period along with increases in blood flow. Because there is little change in metabolic activity for the normal regions, the influx of oxygenated blood flow is likely an overcompensatory response to the damaged tissue.

4.4 Reduced Scattering Coefficient

The μ_s' values at the 650nm wavelength decreased shortly after the burn wound was created (Fig. 7a). Previous research in similar rat burn experiments[29] as well as pig burn experiments[15,16,35] have shown a similar decrease in the μ_s' values in the acute stages of burn wound progression. Additionally they have shown that this decrease is proportional to the severity of the burn. Here we show that this initial decrease in the μ_s' values continue for several days reaching a trough at day 7 for superficial burns and day 14 for deep burns (Fig. 7a) before returning to baseline values. In contrast to the hemodynamic changes seen in the normal areas throughout the experiment, there was no change in μ_s' values at any point during the experiment. This highlights a key difference in what can be measured with these techniques as scattering changes are largely in response to changes in tissue structure. Differences could also be seen in the images of the eschar at day 7 as μ_s' appears relatively uniform (Fig. 7b) compared to the heterogeneity of the relative blood flow changes (Fig. 4b). The presence of the eschar on days 7 and 14 should be considered when analyzing any optical imaging results, as the increased absorption properties will inherently limit the penetration depth of the signal. Using the diffusion approximation[36] to estimate the penetration depth of the light, we found that in the case of the thickest eschar (from the histological measurements) the light was able to penetrate more than three times the thickness of the eschar. While the growth of the eschar on days 7 and 14 will add partial volume measurement errors to data collected at those time points, the majority of the signal still comes from the underlying tissue.

4.5 Water Fraction

Increases in water fraction due to edema are fairly common in burn wounds[37]. Unfortunately, effective fluid resuscitation is a critical component of burn wound care that can often intensify the occurrence of edema[38]. Spectroscopic techniques have been able to quantify increases in water concentration in scar formation[20] and through the formation of

edema with drugs[39]. Acute studies in rat burn models have also shown an increase in relative water fraction over the first 3 hours of burn wounds[29]. Here we also show the ability to track an increase in water fraction shortly after the burns, which remains elevated above baseline conditions throughout the 28 day experiment (Fig. 8b). Being able to accurately monitor tissue water fraction would play a critical role in dictating fluid resuscitation during wound healing as a careful balance must be found between providing enough fluid to the damaged area without giving so much as to exacerbate the presence of edema.

4.6 Future Studies

While it would be interesting to do longer studies in the future to examine the physiology of scar formation similar to what is done in some porcine studies[40], for now we can only speculate what might happen at longer time points based on our data at 28 days. It is possible that elevated oxygenated hemoglobin values could persist for several more weeks while cellular activity is reduced in the maturation phase. It is also possible that the high perfusion values seen in the deep partial thickness burns eventually drop below baseline values (similar to the superficial partial thickness burns at day 28) as blood vessel activity is also reduced. Ultimately, the porcine model is better for studying scarring that is analogous to humans as certain types of scarring, specifically hypertrophic scarring, cannot be recreated in mice and rats[41].

5. Conclusion

SFDI and LSI are both non-invasive modalities that can help discriminate differences in burn severity and quantify different aspects of wound healing over time. These techniques have been used in acute studies to track superficial and deep burns, but here we present those modalities used over 28 days in a hairless rat model. Observed longitudinal changes in scattering and hemodynamics in the burns and surrounding tissue highlight the potential insights that can be gained when studying the different phases of wound healing between burn severities in a rat model. Further development of these methods could aid in monitoring the efficacy of different wound healing treatments.

Acknowledgments

We gratefully acknowledge support from the Arnold and Mabel Beckman Foundation and the NIH, including P41EB015890 (A Biomedical Technology Resource) and UL1 TR000148, and the Military Medical Photonics Program (AFOSR FA9550-14-1-0034). The content is solely the responsibility of the authors and does not necessarily represent the official views of the NIH.

References

1. Peck MD. Epidemiology of burns throughout the world. Part I: Distribution and risk factors. Burns. 2011; 37(7):1087–1100. [PubMed: 21802856]
2. Xiao M, Li L, Li C, et al. Role of autophagy and apoptosis in wound tissue of deep second-degree burn in rats. Academic emergency medicine : official journal of the Society for Academic Emergency Medicine. 2014; 21(4):383–391. [PubMed: 24730400]
3. Kao CC, Garner WL. Acute Burns. Plastic and reconstructive surgery. 2000; 101(7):2482–2493. [PubMed: 11242345]
4. Jackson DM. The diagnosis of the depth of burning. The British journal of surgery. 1953; 40(164): 588–596. [PubMed: 13059343]

5. Shupp JW, Nasabzadeh TJ, Rosenthal DS, Jordan MH, Fidler P, Jeng JC. A review of the local pathophysiologic bases of burn wound progression. Journal of burn care & research : official publication of the American Burn Association. 2010; 31(6):849–873. [PubMed: 21105319]
6. Singh V, Devgan L, Bhat S, Milner SM. The pathogenesis of burn wound conversion. Annals of plastic surgery. 2007; 59(1):109–115. [PubMed: 17589272]
7. Burke-Smith A, Collier J, Jones I. A comparison of non-invasive imaging modalities: Infrared thermography, spectrophotometric intracutaneous analysis and laser Doppler imaging for the assessment of adult burns. Burns. 2015; 41(8):1695–1707. [PubMed: 26421694]
8. Kaiser M, Yafi A, Cinat M, Choi B, Durkin AJ. Noninvasive assessment of burn wound severity using optical technology: a review of current and future modalities. Burns. 2011; 37(3):377–386. [PubMed: 21185123]
9. Hoeksema H, Van de Sijpe K, Tondu T, et al. Accuracy of early burn depth assessment by laser Doppler imaging on different days post burn. Burns. 2009; 35(1):36–45. [PubMed: 18952377]
10. Fourman MS, Phillips BT, Crawford L, et al. Indocyanine green dye angiography accurately predicts survival in the zone of ischemia in a burn comb model. Burns. 2014; 40(5):940–946. [PubMed: 24231464]
11. Prindeze NJ, Hoffman HA, Ardanuy JG, et al. Active Dynamic Thermography is a Sensitive Method for Distinguishing Burn Wound Conversion. Journal of burn care & research : official publication of the American Burn Association. 2015
12. Arbab MH, Winebrenner DP, Dickey TC, Chen A, Klein MB, Mourad PD. Terahertz spectroscopy for the assessment of burn injuries in vivo. Journal of biomedical optics. 2013; 18(7):077004. [PubMed: 23860943]
13. Cuccia DJ, Bevilacqua F, Durkin AJ, Ayers FR, Tromberg BJ. Quantitation and mapping of tissue optical properties using modulated imaging. Journal of biomedical optics. 2009; 14(2):024012. [PubMed: 19405742]
14. Cuccia DJ, Bevilacqua F, Durkin AJ, Tromberg BJ. Modulated imaging: quantitative analysis and tomography of turbid media in the spatial-frequency domain. Optics letters. 2005; 30(11):1354–1356. [PubMed: 15981531]
15. Burmeister DM, Ponticorvo A, Yang B, et al. Utility of spatial frequency domain imaging (SFDI) and laser speckle imaging (LSI) to non-invasively diagnose burn depth in a porcine model. Burns. 2015; 41(6):1242–1252. [PubMed: 26138371]
16. Ponticorvo A, Burmeister DM, Yang B, Choi B, Christy RJ, Durkin AJ. Quantitative assessment of graded burn wounds in a porcine model using spatial frequency domain imaging (SFDI) and laser speckle imaging (LSI). Biomedical optics express. 2014; 5(10):3467–3481. [PubMed: 25360365]
17. Paul DW, Ghassemi P, Ramella-Roman JC, et al. Noninvasive imaging technologies for cutaneous wound assessment: A review. Wound repair and regeneration : official publication of the Wound Healing Society [and] the European Tissue Repair Society. 2015; 23(2):149–162.
18. Rege A, Thakor NV, Rhie K, Pathak AP. In vivo laser speckle imaging reveals microvascular remodeling and hemodynamic changes during wound healing angiogenesis. Angiogenesis. 2012; 15(1):87–98. [PubMed: 22198198]
19. Mirdell R, Iredahl F, Sjoberg F, Farnebo S, Tesselaar E. Microvascular blood flow in scalds in children and its relation to duration of wound healing: A study using laser speckle contrast imaging. Burns. 2016; 42(3):648–654. [PubMed: 26810445]
20. Ghassemi P, Travis TE, Moffatt LT, Shupp JW, Ramella-Roman JC. A polarized multispectral imaging system for quantitative assessment of hypertrophic scars. Biomedical optics express. 2014; 5(10):3337–3354. [PubMed: 25360354]
21. Cuccia, DJ., Abookasis, D., Frostig, RD., Tromberg, BJ. Quantitative In Vivo Imaging of Tissue Absorption, Scattering, and Hemoglobin Concentration in Rat Cortex Using Spatially Modulated Structured Light.. In: Frostig, RD., editor. In Vivo Optical Imaging of Brain Function. 2nd ed.. Boca Raton (FL): 2009.
22. Erickson TA, Mazhar A, Cuccia D, Durkin AJ, Tunnell JW. Lookup-table method for imaging optical properties with structured illumination beyond the diffusion theory regime. Journal of biomedical optics. 2010; 15(3):036013. [PubMed: 20615015]

23. Weber JR, Cuccia DJ, Johnson WR, et al. Multispectral imaging of tissue absorption and scattering using spatial frequency dom ain imaging and a computed-tomography imaging spectrometer. Journal of biomedical optics. 2011; 16(1):011015. [PubMed: 21280902]
24. Crouzet C, Nguyen JQ, Ponticorvo A, Bernal NP, Durkin AJ, Choi B. Acute discrimination between superficial-partial and deep-partial thickness burns in a preclinical model with laser speckle imaging. Burns. 2015; 41(5):1058–1063. [PubMed: 25814299]
25. Ramirez-San-Juan JC, Ramos-Garcia R, Guizar-Iturbide I, Martinez-Niconoff G, Choi B. Impact of velocity distribution assumption on simplified laser speckle imaging equation. Optics express. 2008; 16(5):3197–3203. [PubMed: 18542407]
26. Aguilar G, Choi B, Broekgaarden M, et al. An overview of three promising mechanical, optical, and biochemical engineering approaches to improve selective photothermolysis of refractory port wine stains. Annals of biomedical engineering. 2012; 40(2):486–506. [PubMed: 22016324]
27. Choi B, Ramirez-San-Juan JC, Lotfi J, Stuart Nelson J. Linear response range characterization and in vivo application of laser speckle imaging of blood flow dynamics. Journal of biomedical optics. 2006; 11(4):041129. [PubMed: 16965157]
28. Dunn AK. Laser speckle contrast imaging of cerebral blood flow. Annals of biomedical engineering. 2012; 40(2):367–377. [PubMed: 22109805]
29. Nguyen JQ, Crouzet C, Mai T, et al. Spatial frequency domain imaging of burn wounds in a preclinical model of graded burn sev erity. Journal of biomedical optics. 2013; 18(6):66010. [PubMed: 23764696]
30. Meyerholz DK, Piester TL, Sokolich JC, Zamba GK, Light TD. Morphological parameters for assessment of burn severity in an acute burn injury rat model. Int J Exp Pathol. 2009; 90(1):26–33. [PubMed: 19200248]
31. Ganapathy P, Tamminedi T, Qin Y, et al. Dual-imaging system for burn depth diagnosis. Burns : journal of the International Society for Burn Injuries. 2014; 40(1):67–81. [PubMed: 23790396]
32. Rendell MS, Milliken BK, Finnegan MF, Finney DA, Healy JC. The skin blood flow response in wound healing. Microvascular research. 1997; 53(3):222–234. [PubMed: 9211400]
33. Rendell MS, Johnson ML, Smith D, et al. Skin blood flow response in the rat model of wound healing: expression of vasoactive factors. The Journal of surgical research. 2002; 107(1):18–26. [PubMed: 12384060]
34. Chin MS, Babchenko O, Lujan-Hernandez J, Nobel L, Ignotz R, Lalikos JF. Hyperspectral Imaging for Burn Depth Assessment in an Animal Model. Plastic and reconstructive surgery. Global open. 2015; 3(12):e591.
35. Mazhar A, Saggese S, Pollins AC, Cardwell NL, Nanney L, Cuccia DJ. Noncontact imaging of burn depth and extent in a porcine model using spatial frequency domain imaging. Journal of biomedical optics. 2014; 19(8):086019. [PubMed: 25147961]
36. Jacques SL, Pogue BW. Tutorial on diffuse light transport. Journal of biomedical optics. 2008; 13(4):041302. [PubMed: 19021310]
37. Lund T, Onarheim H, Reed RK. Pathogenesis of edema formation in burn injuries. World journal of surgery. 1992; 16(1):2–9. [PubMed: 1290261]
38. Kompoti MG, Michalia MG. Critical care of the burn patient: the first 48 hours. Critical care medicine. 2010; 38(5):1391. author reply 1391-1392. [PubMed: 20404643]
39. Stamatas GN, Southall M, Kollias N. In vivo monitoring of cutaneous edema using spectral imaging in the visible and near infrared. The Journal of investigative dermatology. 2006; 126(8): 1753–1760. [PubMed: 16675964]
40. Rapp SJ, Rumberg A, Visscher M, Billmire DA, Schwentker AS, Pan BS. Establishing a Reproducible Hypertrophic Scar following Thermal Injury: A Porcine Model. Plastic and reconstructive surgery. Global open. 2015; 3(2):e309.
41. Zhu KQ, Carrougher GJ, Gibran NS, Isik FF, Engrav LH. Review of the female Duroc/Yorkshire pig model of human fibroproliferative scarring. Wound repair and regeneration : official publication of the Wound Healing Society [and] the European Tissue Repair Society. 2007; 15(Suppl 1):S32–39.

a)

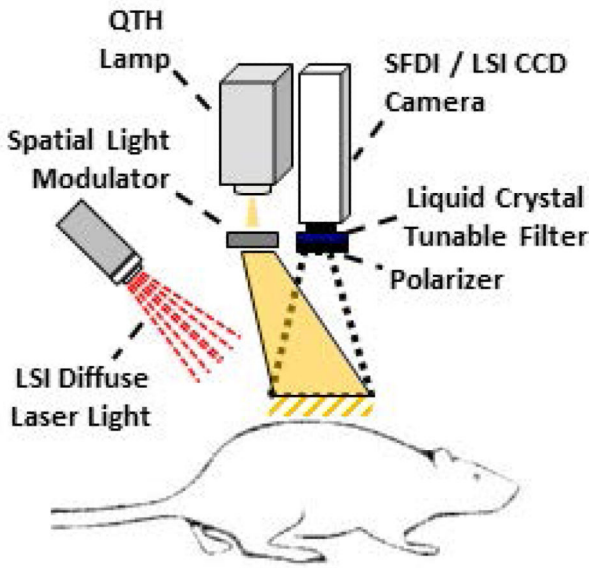

b)

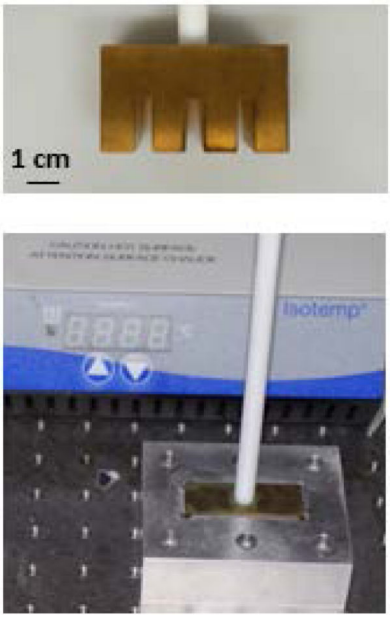

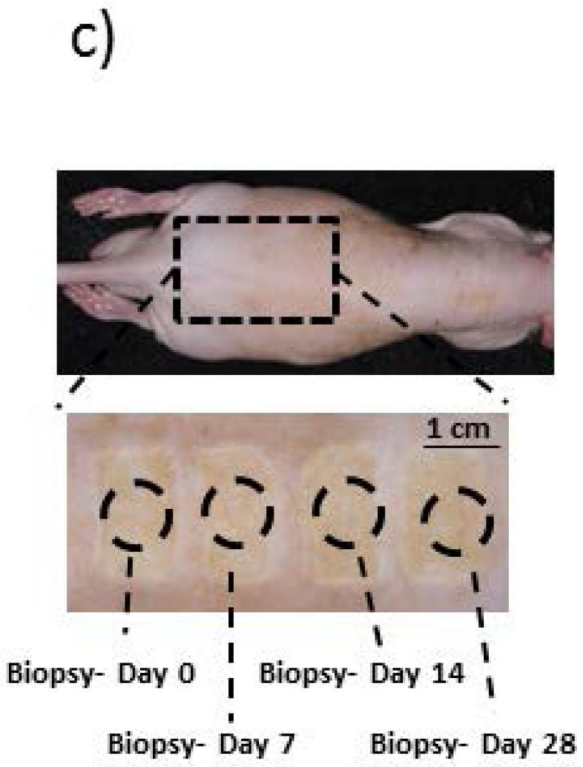

Fig. 1.

a) A schematic of the SFDI and LSI setup. b) An image of the burn tool and incubator. c) An image of the burn site on a CD hairless rat. Biopsy sites are shown with dashed circles.

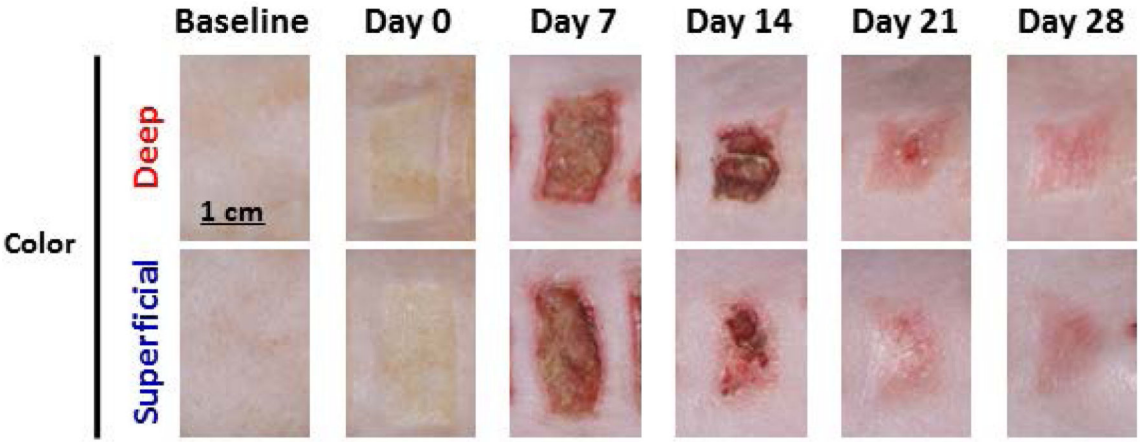

Fig. 2.

A time series of color images taken from a representative superficial and deep burn.

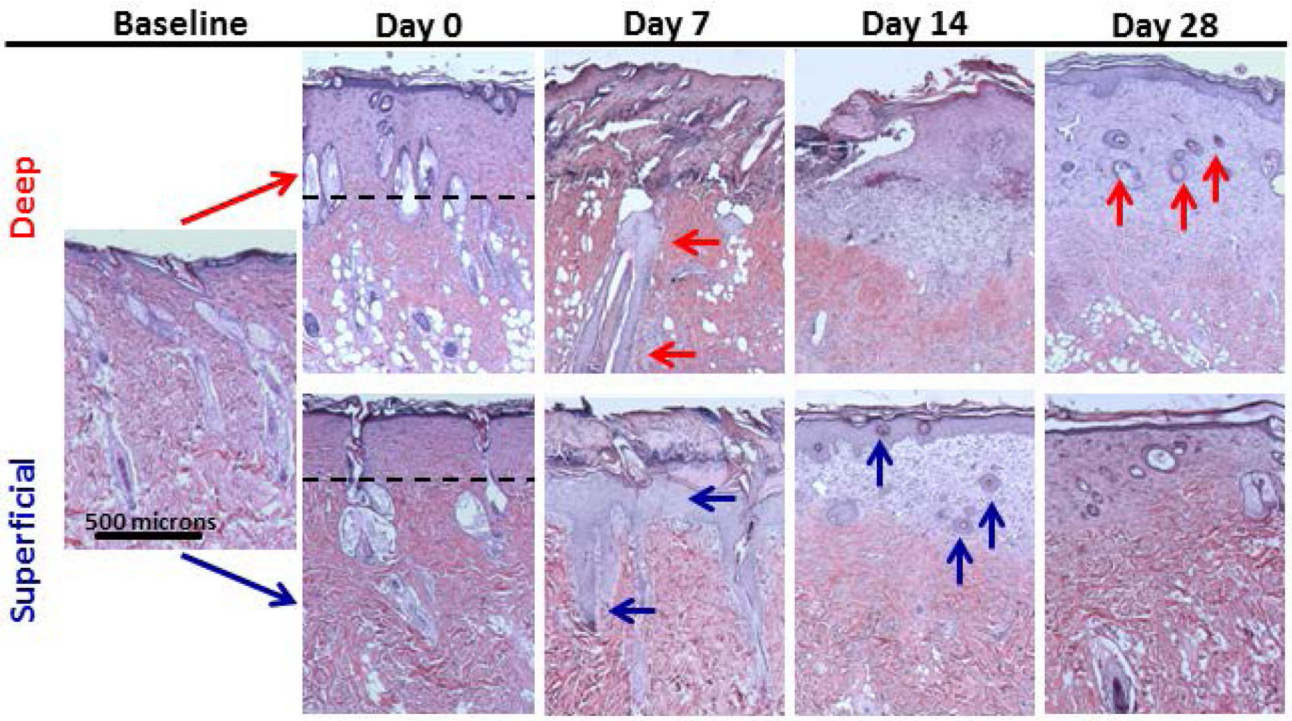

Fig. 3.

Histology images representing baseline, days 0, 7, 14, and 28. Burn depth is represented by dotted lines on the day 0 sample. On day 7, Re-epithelialization starts from the undamaged hair follicle in the superficial burns (blue arrows), but only originates from the bulge of damaged hair follicles in deep burns (red arrows). New hair follicles are present in the superficial burns by day 14 (blue arrows), but are not as apparent in the deep burns until day 28 (red arrows).

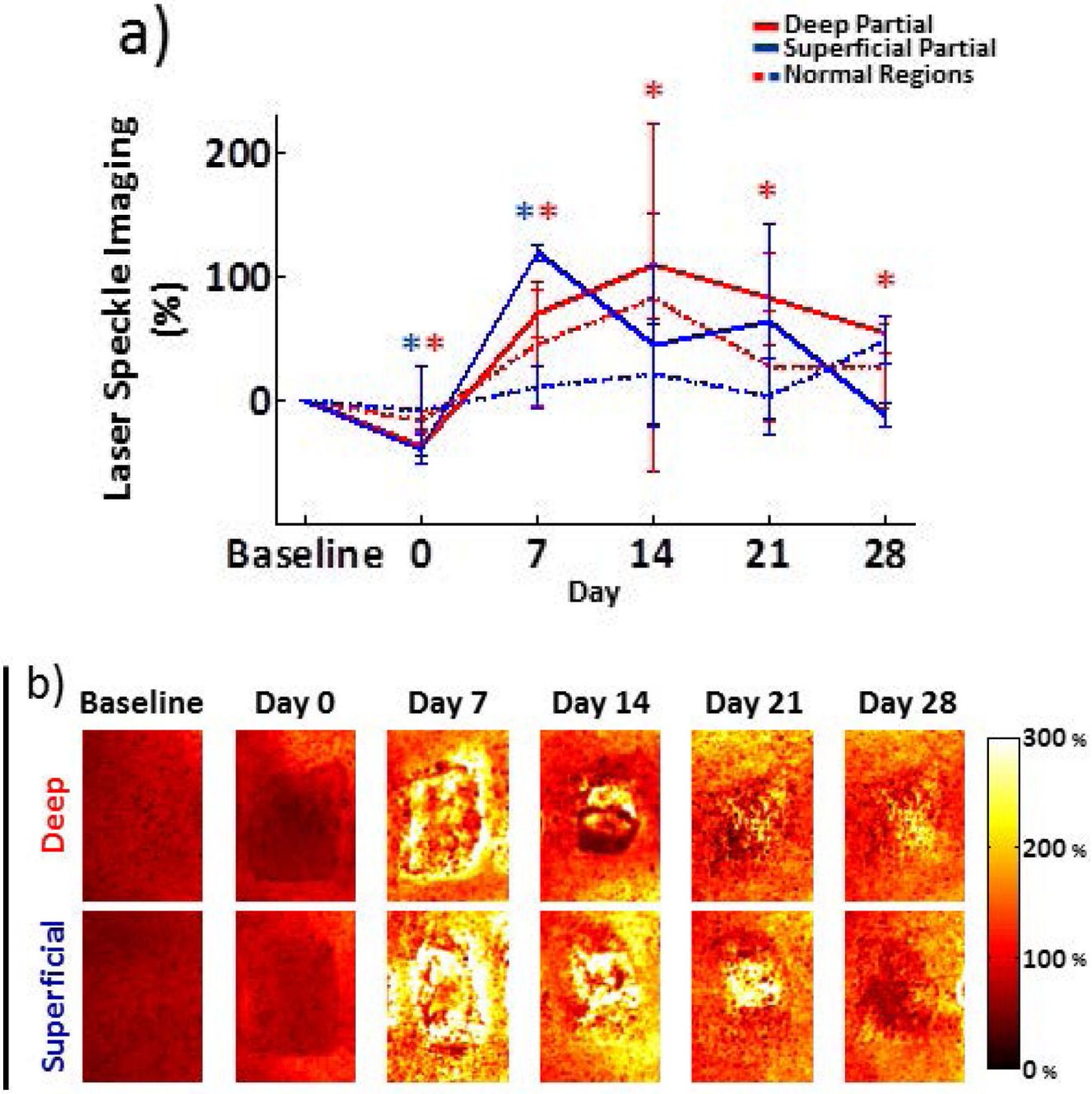

Fig. 4.

a) Time course of relative changes in the speckle flow index. The asterisks denote relative LSI values that differ significantly between the burn wounds and the baseline conditions. b) Relative blood flow images derived from LSI for a representative deep and superficial burn.

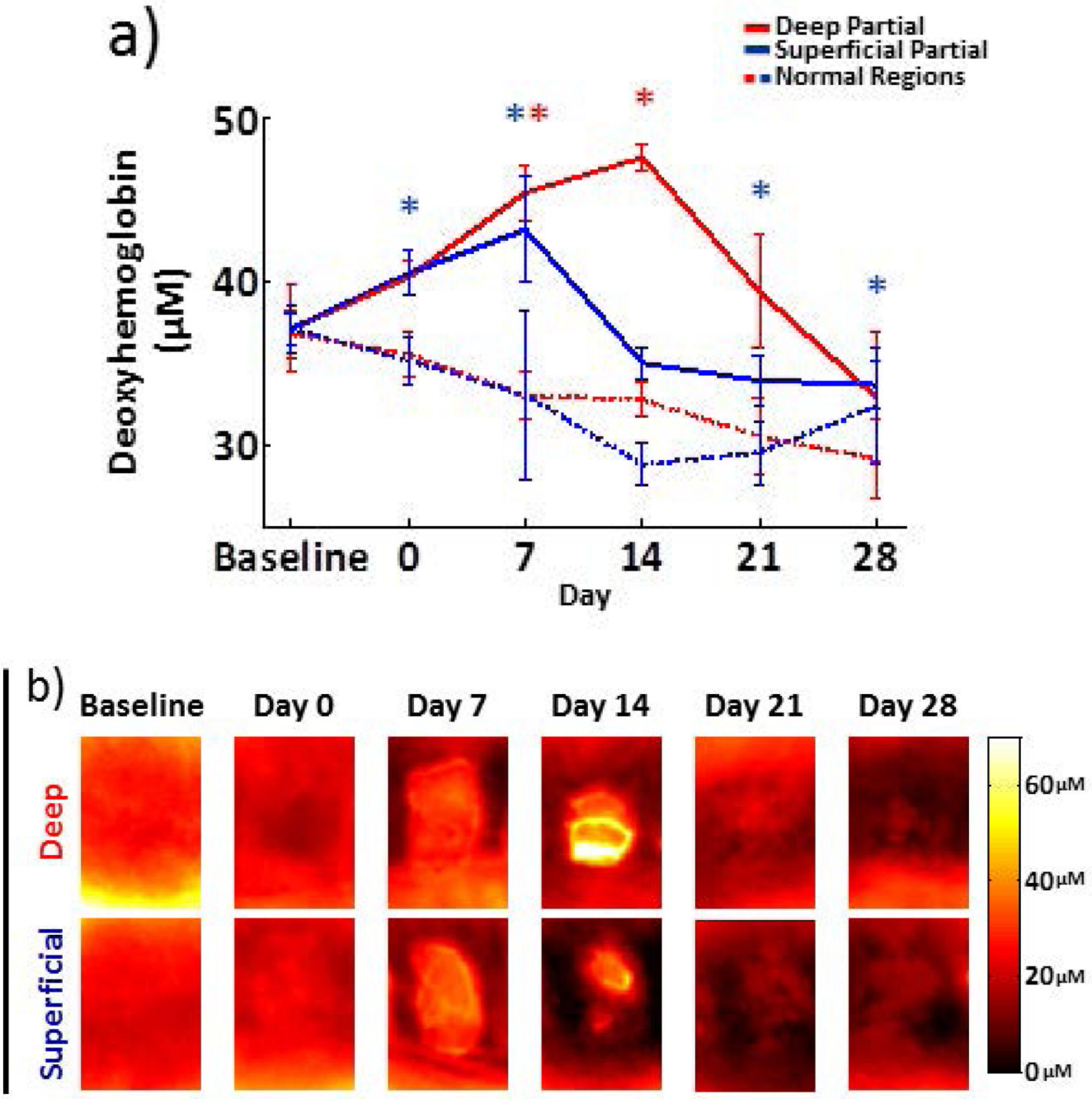

Fig. 5.

a) Time course of deoxygenated hemoglobin concentrations. The asterisks denote deoxygenated hemoglobin concentrations that differ significantly between the burn wounds and the baseline conditions. b) Representative deoxygenated hemoglobin concentrations images derived from SFDI for a deep and superficial burn.

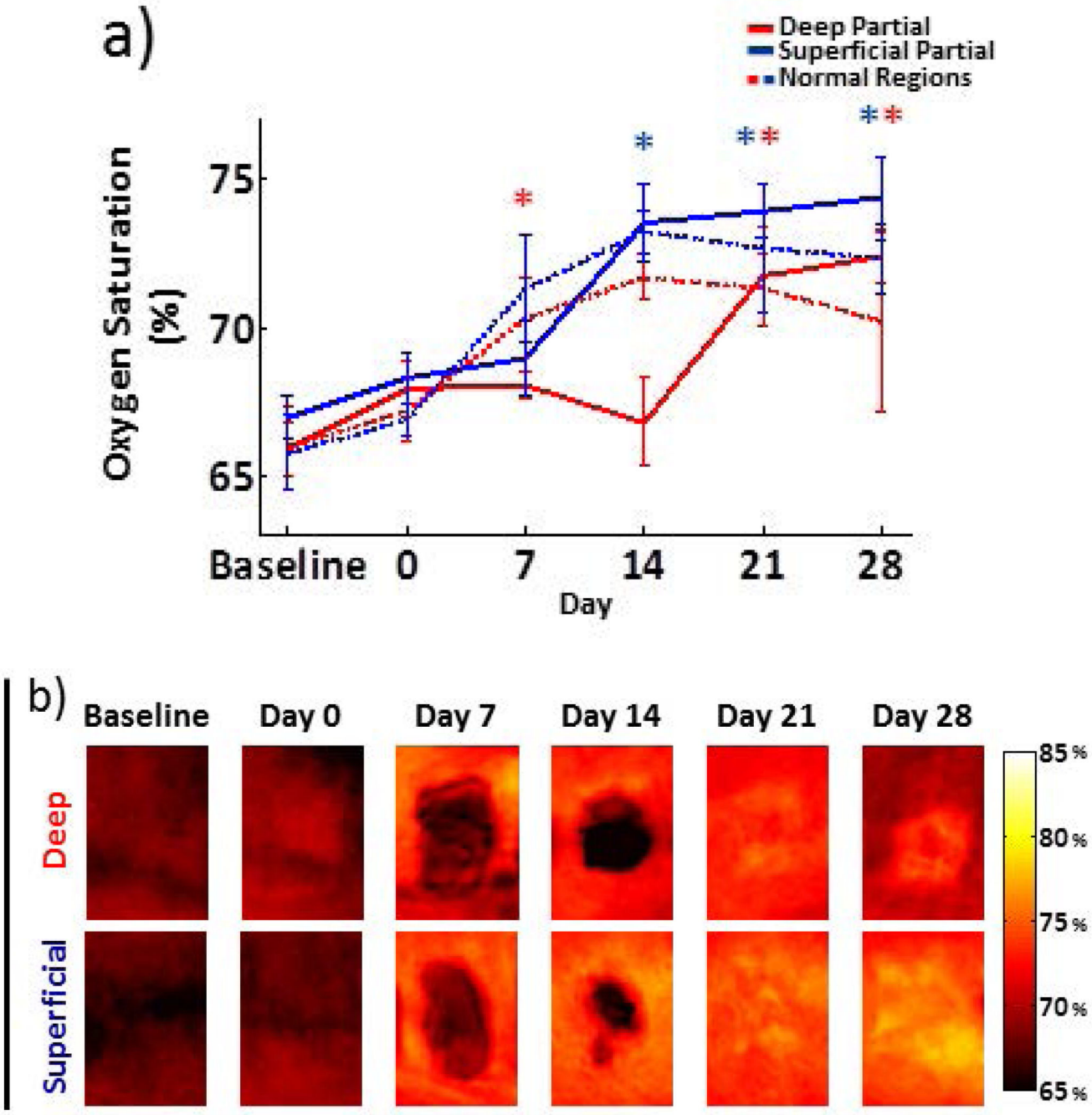

Fig. 6.

a) Time course of oxygen saturation values. The asterisks denote oxygen saturation values that differ significantly between the burn wounds and the baseline conditions. b) Representative oxygen saturation images derived from SFDI for a deep and superficial burn.

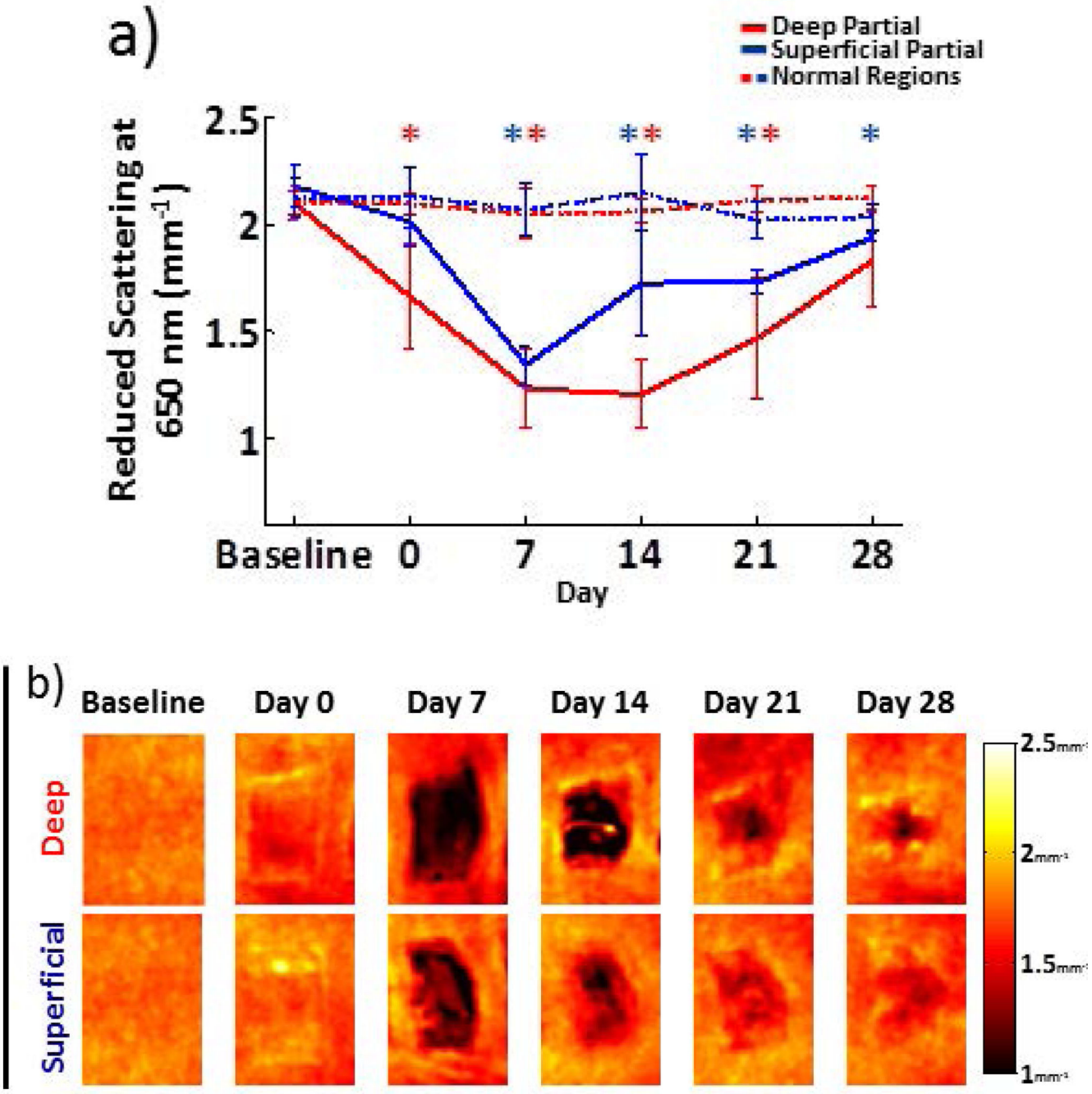

Fig. 7.

a) Time course of μ_s' at 650nm values. The asterisks denote μ_s' values that differ significantly between the burn wounds and the baseline conditions. b) Representative μ_s' images derived from SFDI for a deep and superficial burn.

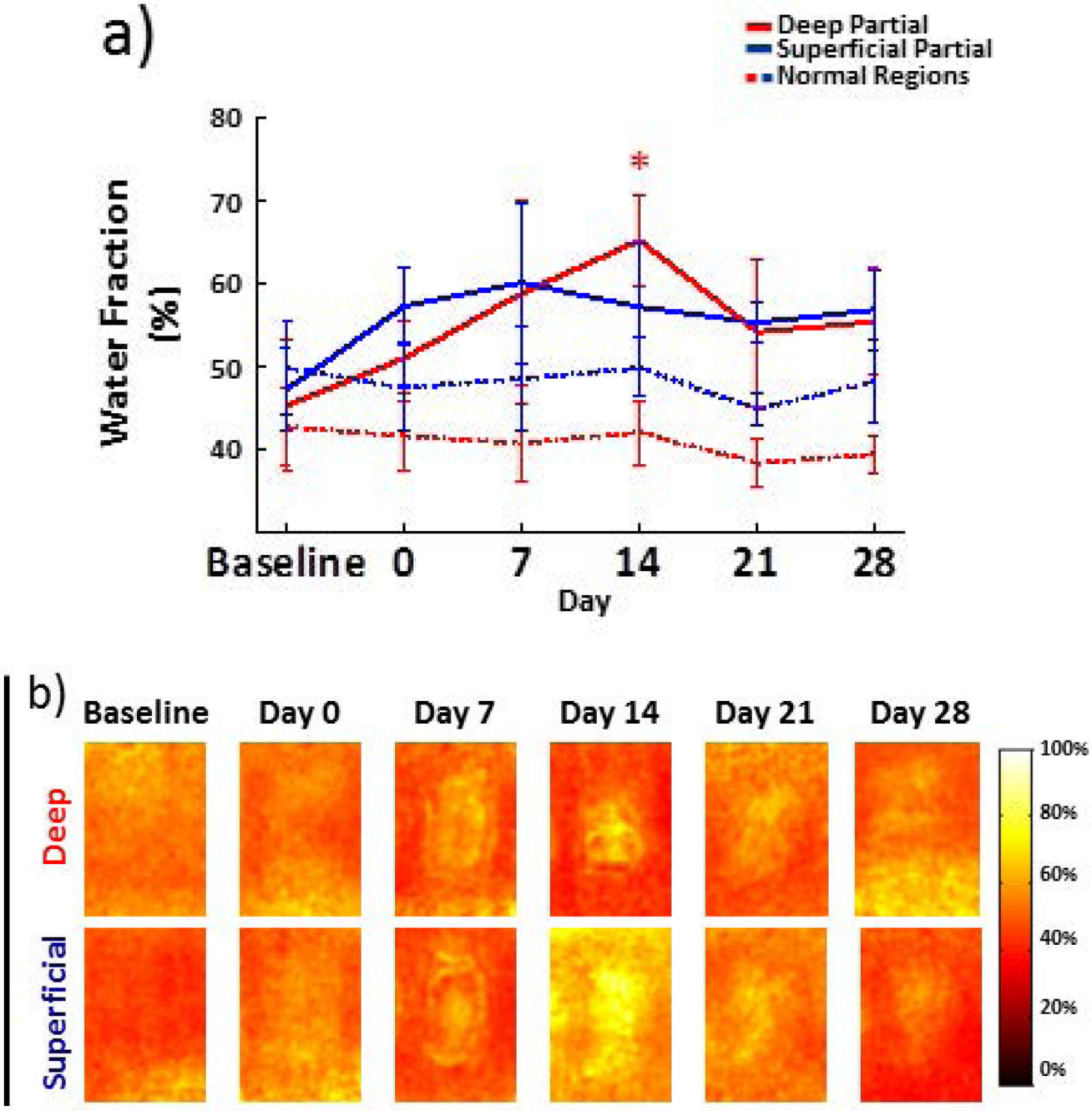

Fig. 8.

a) Time course of water fraction changes. The asterisks denote water fraction values that differ significantly between the burn wounds and the baseline conditions. b) Representative water fraction images derived from SFDI for a deep and superficial burn.

Table 1

Summary of the LSI and SFDI parameters.

	Baseline		Day 0		Day 7		Day 14		Day 21		Day 28	
Parameter	**SP**	**DP**	**SP**	**DP**	**SP**	**DP**	**SP**	**DP**	**SP**	**DP**	**SP**	**DP**
μ_s‘ (mm^{-1})	2.18	2.10	2.01	1.66*	1.34*	1.23*	1.73*	1.21*	1.73*	1.47*	1.94*	1.84
Blood Flow (%)	100	100	60*	64*	220*	166*	145	210*	164	172*	88	154*
stO_2 (%)	67	66	68	68	68	68	73*	70	74*	72*	74*	73*
HbO_2 (μM)	75	73	86*	85*	93*	96*	93*	106*	96*	101*	98*	84
Hb (μM)	37	37	41*	40	43*	45*	35	46*	34*	40	34*	33
H_2O (%)	47	45	57	51	60	59	57	65*	55	54	57	55